doi 10.26089/NumMet.v21r109

SIMULATION OF UNSTEADY GAS-PARTICLE FLOW INDUCED BY THE SHOCK-WAVE INTERACTION WITH A PARTICLE LAYER

K. N. Volkov[1], V. N. Emelyanov[2], A. G. Karpenko[3], I. V. Teterina[4]

A numerical simulation of the unsteady gas-particle flow arising from the shock-wave interaction with a layer of inert particles is performed based on a continuum model. Each phase is described by a set of equations describing the conservation laws of mass, momentum and energy. The interphase interaction is taken into account using source terms in the momentum and energy equations. The governing equations for the gas and dispersed phases are of a hyperbolic type, they are written in a conservative form and are solved with a Godunov type numerical method. A third order Runge–Kutta method is used to discretize the governing equations in time. The proposed model allows one to calculate a wide range of gas-particle flow regimes occurring when the volume concentration of the dispersed phase varies. The closure of the mathematical model and some details of numerical model implementation are discussed. The shock-wave flow structure as well as the space-time dependencies of particle concentration and other flow parameters are presented.

Keywords: two-phase flow, numerical simulation, shock wave, particle, concentration

1. Introduction. Mathematical simulation of multiphase media flows is a topic of interest to many scientific disciplines and engineering applications. A multiphase medium is usually understood as a continuous medium consisting of several components (phases) with different physical properties. Despite the high demand for this topic, many issues related to building physical, mathematical and computational models of multiphase flows require further research [1].

It is quite common for practical applications in the field of gas dynamics to require taking into account additional physical factors and processes. This requires introducing new components into the gas dynamics equations and adding extra equations and calculations to the system, which changes the content of mathematical models. In gas-particle mixtures, the flow pattern is described by the influence of relaxation processes in the velocities and temperatures of the two phases, the typical lengths of which are determined by the particle size.

In the interpenetrating continuum model proposed in [2], the multiphase flow is considered as a set of interacting continuums (phases) and is described by the parameters obtained by applying the filtering procedure. The behavior of each phase is described by the laws of mass, momentum and energy conservation, while interaction between the phases is taken into account by adding special algebraic or differential terms to the right-hand side of the conservation law equations. One problem with the classical models obtained by the filtering method is the challenge of properly describing the processes taking place at the boundary between phases.

A common approach to describing the flows in two-phase compressible media is the use of single pressure models. Usually the systems of equations used in models like this are of a mixed elliptic and hyperbolic type, which makes it difficult to set the initial boundary value problems properly [3]. To overcome the challenges associated with the improper setting of the initial boundary value problem, various modifications of the single pressure model are proposed [4]. The hyperbolicity of the basic equations in such models is achieved by introducing additional differential summation terms in the right-hand side of the equations describing changes

[1] Ustinov Baltic State Technical University. Faculty of Rocket and Space Engineering; ulitsa Pervaya Krasnoarmeiskaya 1, St. Petersburg, 190005, Russia, e-mail: dsci@mail.ru

[2] Ustinov Baltic State Technical University. Faculty of Rocket and Space Engineering; ulitsa Pervaya Krasnoarmeiskaya 1, St. Petersburg, 190005, Russia, e-mail: vlademelyanov@gmail.com

[3] St. Petersburg State University. Faculty of Mathematics and Mechanics; Universitetskii prospekt 28, St. Petersburg, 198504, Russia, e-mail: aspera.2003.ru@mail.ru

[4] Ustinov Baltic State Technical University. Faculty of Rocket and Space Engineering; ulitsa Pervaya Krasnoarmeiskaya 1, St. Petersburg, 190005, Russia, e-mail: yaiv@mail.ru

© Research Computing Center Lomonosov Moscow State University

in the quantity of motion, which are called virtual mass forces and interphase pressure. This results in a hyperbolic system of basic equations; however, reducing it to a symmetric form or representing all the equations in the system in a divergence form becomes impossible. This complicates the application of modified models for the study of discontinuous solutions, including problems involving shock waves and contact discontinuities.

The phenomenological model of interpenetrating continuums has historically been one of the first models designed to calculate the flows in two-phase media. A study of the propriety of the Cauchy problem for a system of equations describing the flow of gas with particles is carried out for the case of unsteady one-dimensional flow of gas suspension with and without the particle volume taken into account [5]. The Cauchy problem is generally improper for calculating the flow of gas-particle mixture [6]. With some small initial disturbances, the concentration of disperse phase becomes infinitely large, which in a two-velocity model is associated with the intersection of particle trajectories.

Intersection of the particle trajectories (or streamlines of the particles in the pseudo-gas given a stationary flow) leads to two or more different velocity vectors of the dispersed phase being present at the intersection of the particle trajectories. This leads to ambivalence of the dispersed phase parameter fields (violation of unique solution principle) and to the emergence of special surfaces (folds or caustic fields) in the flowfield, on which the particle concentration increases sharply or infinitely [7]. The perturbations of other parameters (pressure, velocity, etc) remain in the vicinity of their initial values.

The source of non-hyperbolicity lies in the lack of internal pressure in the dispersed phase [5]. In order to eliminate non-hyperbolicity (while preserving the two-veelocity gas suspension model), additional artificial pressure is introduced in the momentum change equation for the dispersed phase, which prevents non-physical increases in particle concentration. In the actual flow, particle pressure in the pseudo-gas is created due to interaction between the particles and chaotic particle movement. The instability of numerical solutions is an inherent property of the interpenetrating continuums model, caused by an insufficient description of interaction between the phases and interactions within the dispersed phase.

It is quite difficult to take into account the factors contributing to the admixture chaotic movement within the framework of the phenomenological model of interpenetrating continuums. Ignoring the random factors helps simplify the two-phase flow model, but that means the numerical schemes developed for solving the problems of classical gas dynamics are no longer usable. Ignoring interactions between the particles, such as collisions, turns the dispersed pseudo-gas into a medium without internal pressure.

In the two-pressure model proposed in [8] (Baer–Nunziato model), the two media composing the two-phase mixture are described by their own systems of conservation laws, while phase interaction is simulated by special terms in the right-hand side of the continuity and momentum change equations. Speed and pressure values at the boundary of the two phases are selected in different ways depending on the model area of application. For gaseous media containing solid particles, the boundary speed value is assumed to equal the speed of the solid phase, and the boundary pressure value is assumed to equal the gas pressure value. In a three-dimensional case, the Baer–Nunziato equations are a system of 11 differential equations with partial differentials (5 for the gas phase and 6 for the solid phase).

In [9], a non-equilibrium two-fluid model is used to describe the motion of a compressible multiphase mixture with phase boundaries, completed by a volume concentration equation. Despite the fact that hyperbolic equations are used in the simulation, not all of them are presentable in a divergence form, which causes difficulties when attempting to simulate discontinuous solutions, and complicates the use of modern computational methods.

Mathematical features of the single-dimensional Baer–Nunziato equations are investigated in [10]. The Baer–Nunziato equations are hyperbolic, but they cannot be written in the form of conservation laws (in a divergence form). When recorded using conservative variables, the equations retain non-conservative terms, which renders it impossible to apply the classical Rankine–Hugoniot conditions to discontinuities. Solving the non-conservative hyperbolic equations is a challenging task from both theoretical and computational points of view [11, 12, 13]. Riemann problem for the Baer–Nunziato equations is formulated and solved in [14, 15, 16, 17]. Given certain initial data, Riemann problem can have more than one solution [18]. An approximation of the Riemann problem is used to build a numerical flow for the conservative part of the equations. The Roe scheme is applied in [17], and numerical approaches to solving the Baer–Nunziato equations based on the finite volume method and Galerkin method with discontinuous basic functions are developed in [19, 20, 21].

In a general case, six families of undulations are present in the task: three for the gas phase and three for the solid phase. Six characteristics divide the (x, t) plane into seven sub-planes, within which the medium maintains

stable parameters. Solid phase variables remain stable when crossing all three gas characteristic undulations, while the contact discontinuities in the solid phase change all gas variables except tangential velocity. The left and right non-linear solid phase undulations do not affect the gas variables, and the phase concentration leap only occurs at the contact discontinuity of the solid phase. In the vicinity of the contact discontinuity of the solid phase, the right part of the Baer–Nunziato equations becomes non-zero, and the equations for both phases become bound due to the concentration leap. The classical Rankine–Hugoniot conditions become inapplicable, and therefore the contact discontinuity in the solid phase is considered as an infinitely thin layer in which all gas parameters change continuously and all differentials exist [15]. Thin layer equations bind medium parameters on both sides of the contact discontinuity of the solid phase.

A statistical approach based on a kinetic equation for the probability density function of particle velocities represents a sequential method for building continuous models of gas suspension flows. Statistical models of two-phase flows are considered in [22, 23]. The movement of disperse phase is described in the framework of a continuum approach, based on the application of the Liouville theorem to the system of dynamic equations describing the behavior of an individual particle [24]. The influence of sub-grid effects on the motion of particles in a turbulent flow is discussed in [25, 26] in the framework of the interpenetrating continuum model. Despite numerous studies, there is no universally accepted approach to mathematical modelling of multiphase compressible flows. The existing approaches have weaknesses related to non-hyperbolic nature of the equation system and the presence of equations that cannot be represented in a divergence form. Satisfying the above requirements provides a mathematical basis for setting initial boundary value problems, and opens up opportunities for the development of numerical algorithms.

This paper develops a model designed for numerical simulation of unsteady gas flows with inert particles. Introducing the probability density function allows formulating a statistical description of the particle system instead of giving a dynamic description of individual particles based on the Langevin stochastic equation. The continuity, momentum and energy change equations for the gas and disperse phases are hyperbolic in nature and are solved using the Godunov-type numerical scheme at an increased order of accuracy. Flow structure and spatial and temporal dependencies of flow parameters at interaction with a layer of particles of subsonic and supersonic flow speeds are calculated.

2. Mathematical model. Equations describing the motion and heat transfer in the dispersed phase are derived from the Liouville equation describing the probability density function of particle distribution by coordinates, velocities and temperatures. To complete the resulting equations, the correlation moments of velocity and temperature in the dispersed phase are ignored. When recording the basic equations, indices g and p correspond to gas and particles.

2.1. The discrete model. The motion and heat transfer equations for a sample particle are stochastic Langevin-type equations depending on the random velocity $\boldsymbol{v}_g$ and temperature T_g fields of the carrier flow, where the velocity and temperature of the carrier gas are calculated at various points along the particle trajectory. The equations describing motion and heat transfer for a sample particle are of the form

$$\frac{d\boldsymbol{x}_p}{dt} = \boldsymbol{v}_p; \tag{1}$$

$$m_p \frac{d\boldsymbol{v}_p}{dt} = \boldsymbol{f}_p; \tag{2}$$

$$c_p^m m_p \frac{dT_p}{dt} = q_p. \tag{3}$$

Here, m_p is the particle mass; c_p^m is the heat capacity of particle material; $\boldsymbol{x}_p$ is the position vector of the particle center of mass; $\boldsymbol{v}_p$ is the particle speed; T_p is the particle temperature; $\boldsymbol{f}_p$ is the force acting upon the particle; q_p is the convective heat flow between gas and the particle.

For the drag force acting on the particle, the ratio is

$$\boldsymbol{f}_p = \frac{1}{2} C_D \rho_g \left|\boldsymbol{v}_g - \boldsymbol{v}_p\right| (\boldsymbol{v}_g - \boldsymbol{v}_p) S_m,$$

where ρ is the density, and S_m is the mid-section area of the particle. The resistance factor is presented as

$$C_D = C_{D0} f_D,$$

where $C_{D0} = 24/\mathrm{Re}_p$ is the drag coefficient corresponding to the Stokes law; f_D is a function adjusting for

particle inertia and compressibility. The correction function is represented as

$$f_D = \left(1 + 0.15\mathrm{Re}_p^{0.687}\right)\left[1 + \exp\left(-\frac{0.427}{\mathrm{M}_p^{4.63}} - \frac{3}{\mathrm{Re}_p^{0.88}}\right)\right].$$

Reynolds and Mach numbers are calculated from the relative velocity of gas and particles

$$\mathrm{Re}_p = \frac{2\rho_g r_p\,|\boldsymbol{v}_g - \boldsymbol{v}_p|}{\mu}, \quad \mathrm{M}_p = \frac{|\boldsymbol{v}_g - \boldsymbol{v}_p|}{c},$$

where μ is dynamic viscosity, and c is local speed of sound. For a spherical particle with radius r_p the mid-section area is $S_m = \pi r_p^2$ and $m_p = 4\pi r_p^3\rho_p/3$. Equation (2) is presented as

$$\frac{d\boldsymbol{v}_p}{dt} = \frac{f_D}{\tau_v}(\boldsymbol{v}_g - \boldsymbol{v}_p). \tag{4}$$

Here, $\tau_v = \rho_p d_p^2/(18\mu)$ is the dynamic relaxation time.

Expressing the heat transfer factor through the Nusselt number ($h = \mathrm{Nu}_p\lambda_p/d_p$), the convective heat flux between the gas and the particle is presented in the form

$$q_p = \mathrm{Nu}_p\lambda(T_g - T_p)\frac{S_p}{d_p},$$

where S_p is the particle surface area, and λ is the heat conductivity of the gas. The Nusselt number is presented in a form adjusted for particle inertia

$$\mathrm{Nu}_p = 2 + 0.459\mathrm{Re}_p^{0.55}\mathrm{Pr}^{0.33},$$

where Pr is the Prandtl number (Pr = 0.72 for air). Equation (3) is presented as

$$\frac{dT_p}{dt} = \frac{1}{\tau_\vartheta}(T_g - T_p), \tag{5}$$

where $\tau_\vartheta = c_p\rho_p d_p/(3\lambda\mathrm{Nu}_p)$ is the thermal relaxation time, and $\tau_\vartheta = (3\mathrm{Pr}\beta/\mathrm{Nu}_p)\tau_v$, where $\beta = c_p^m/c_p$ is the ratio of specific heat capacity of the dispersed phase to specific heat capacity of the gas at constant pressure.

In non-dimensional variables, dynamic and thermal relaxation times are replaced by Stokes numbers

$$\mathrm{Stk}_v = \frac{2\rho_p r_p^2 U}{9\mu L}, \quad \mathrm{Stk}_\vartheta = \frac{2c_p\rho_p r_p U}{3\lambda\mathrm{Nu}_p L},$$

where L and U are characteristic length and velocity scales.

2.2. The continuity model. The approach proposed in [22] for large-eddy simulation of turbulent gas suspension flows, and its generalization developed in [25, 26] for direct numerical simulation of two-phase flows are used to construct equations describing motion and heat transfer in the particle continuum. In the continuum approach, the continuity equation, momentum equation and energy equation of the dispersed phase are derived from the Lagrangian equations of motion and heat transfer of an individual particle recorded in (1), (4) and (5). For simplicity, it is assumed that $f_D = 1$ and $\mathrm{Nu}_p = 2$.

To make transfer from the dynamic stochastic Langevin-type equations (Lagrangian description) to a statistical description of the particle system distribution by coordinates, velocities and temperatures (Euler description), the dynamic density of the probability distribution in the phase space of the particle coordinates, velocities and temperatures is introduced

$$w_i(\boldsymbol{x}_p, \boldsymbol{v}_p, \vartheta_p, t) = \delta\Big[\boldsymbol{x}_p - \boldsymbol{x}_{pi}(t)\Big]\delta\Big[\boldsymbol{v}_p - \boldsymbol{v}_{pi}(t)\Big]\delta\Big[\vartheta_p - \vartheta_{pi}(t)\Big],$$

where $\boldsymbol{v}_p$, ϑ_p are the velocity and temperature of the dispersed phase, representing a manifestation of a random velocity and temperature field at time t in point $\boldsymbol{x}_p$; $\boldsymbol{v}_{pi}$, ϑ_{pi} are parameters acting as independent variables.

At time t, the state of a system consisting of N particles is determined by setting the coordinates $\boldsymbol{x}_{p1}, \ldots, \boldsymbol{x}_{pN}$, velocities $\boldsymbol{v}_{p1}, \ldots, \boldsymbol{v}_{pN}$ and temperatures $\vartheta_{p1}, \ldots, \vartheta_{pN}$ of all particles. The aggregate of coordinates, velocities and temperatures of an individual particle is expressed as $\boldsymbol{z}_{pi} = (\boldsymbol{x}_{pi}, \boldsymbol{v}_{pi}, \vartheta_{pi})$, where

$i = 1, \ldots, N$, and the aggregate of coordinates, velocities and temperatures of all particles in the system is expressed as $Z = (\boldsymbol{x}_{p1}, \ldots, \boldsymbol{z}_{pN})$.

Considering particles as statistically independent units, the single-point dynamic density of probability distribution is defined

$$w(\boldsymbol{x}_p, \boldsymbol{v}_p, \vartheta_p, t) = \frac{V_p}{V_\Sigma} \sum_{i=1}^{N} w_i(\boldsymbol{x}_p, \boldsymbol{v}_p, \vartheta_p, t),$$

where V_p is the particle volume, and V_Σ is the system volume. The local functions of the dynamic variables, which depend on the position of the point $z_p = z_p(\boldsymbol{x}_p, \boldsymbol{v}_p, \vartheta_p)$ in the phase space, are expressed through the microscopic phase density in the coordinate space, velocities and temperatures of the particles, which meets the normalization condition

$$\int w(\boldsymbol{x}_p, \boldsymbol{v}_p, \vartheta_p, \tau) d\boldsymbol{x}_p d\boldsymbol{v}_p d\vartheta_p = 1.$$

Assuming $z_p = (\boldsymbol{x}_p, \boldsymbol{v}_p, \vartheta_p)$ and $z_{pi} = (\boldsymbol{x}_{pi}, \boldsymbol{v}_{pi}, \vartheta_{pi})$, the following expression is derived

$$w(x, t) = \sum_{i=1}^{N} \delta\Big[z_p - z_{pi}(t)\Big].$$

The distribution of macroscopic states of the system evolves as a result of changes in the location of points $z_{p1}, \ldots, z_{pN}$, which describe the system state at different points in time. By differentiating the dynamic density of the probability distribution in phase space over time, using the equations of momentum and heat transfer equations for a sample particle recorded in Lagrangian variables, and by summing over $i = 1, \ldots, N$, the stochastic Liouville equation is derived [22, 27]

$$\frac{\partial W}{\partial t} + \frac{\partial}{\partial x_i}(v_i W) - \frac{\partial}{\partial v_i}\left(\frac{v_i - u_i}{\tau_v} W\right) - \frac{\partial}{\partial \vartheta}\left(\frac{\vartheta - T}{\tau_\vartheta} W\right) = 0, \tag{6}$$

where x_i, v_i and ϑ are the coordinates, velocity and temperature of the particle, respectively. Summation by repeating indices is assumed.

The spatial filtering operator is defined by the ratio

$$\overline{f}(\boldsymbol{x}) = \int f(\boldsymbol{\xi}) H_\Delta(\boldsymbol{x} - \boldsymbol{\xi}) d\boldsymbol{\xi},$$

where $\overline{f}$ is the average value of the f function, H_Δ is the kernel function. The kernel is non-negative and meets the normalization criteria. The filter width Δ is set small enough, so that the ratio $\widetilde{\boldsymbol{v}}_g = \boldsymbol{v}_g$ is true for the gaseous phase. Gas variable are not affected by sub-grid fluctuations, therefore $\widetilde{u_i W} = u_i \widetilde{W}$ and $\widetilde{TW} = T\widetilde{W}$. Given a non-negative kernel (top-hat filter, Gaussian filter), the function $\overline{W}$ meets the requirements to the probability density function [28, 29].

Let's assume Z is the aggregate of coordinates, velocities and temperatures of all particles in the system, while $\mathcal{Z}$ is the aggregate of spatial coordinates, velocities and temperatures in phase space. Along with the probability distribution density of the states of the particle system $\delta[\mathcal{Z} - Z(t)]$, let's introduce the average probability distribution density of the system states $\overline{W}(\mathcal{Z}, t)$. It follows from the definition of the filtering operation that

$$\widetilde{\boldsymbol{v}_{pi} w} = \boldsymbol{v}\overline{W}, \quad \widetilde{\vartheta_{pi} w} = \vartheta \overline{W}.$$

By averaging the Liouville equation over the ensemble of random implementations of velocity and temperature fields, a statistical description of the particle system is derived. By applying the filtering operator to equation (6), the filtering Liouville equation is obtained

$$\frac{\partial \overline{W}}{\partial t} + \frac{\partial}{\partial x_i}\left(v_i \overline{W}\right) - \frac{\partial}{\partial v_i}\left(\frac{v_i - u_i}{\tau_v} \overline{W}\right) - \frac{\partial}{\partial \vartheta}\left(\frac{\vartheta - T}{\tau_\vartheta} \overline{W}\right) = 0. \tag{7}$$

Liouville stochastic equation, because of its linearity, has the same form for functions $W(\mathcal{Z},t)$ and $\overline{W}(\mathcal{Z},t)$. The average numerical concentration $\widetilde{\alpha}$ (particle number density), average velocity $\widetilde{v}_i$ and average temperature $\widetilde{\vartheta}$ of the dispersed phase are derived from ratios

$$\widetilde{\alpha}(\boldsymbol{x},t)=\int\overline{W}(\boldsymbol{x},\boldsymbol{v},\vartheta,t)d\boldsymbol{v}d\vartheta;$$
$$\widetilde{v}_i(\boldsymbol{x},t)=\frac{1}{\widetilde{\alpha}}\int v_i\overline{W}(\boldsymbol{x},\boldsymbol{v},\vartheta,t)d\boldsymbol{v}d\vartheta;$$
$$\widetilde{\vartheta}(\boldsymbol{x},t)=\frac{1}{\widetilde{\alpha}}\int\vartheta\overline{W}(\boldsymbol{x},\boldsymbol{v},\vartheta,t)d\boldsymbol{v}d\vartheta.$$

Equation (7) allows deriving equations for the linear and quadric moments of the disperse phase. The single-point momentum transfer equations describing oscillatory qualities of the disperse phase are derived by multiplying the kinetic equation by the weighting function, with subsequent integration over the subspace of phase velocities.

First-order moments represent average values of the dynamic gas flow parameters, depending on the spatial and temporal position of the point. Linear moment equations have the following form

$$\frac{\partial\widetilde{\alpha}}{\partial t}+\frac{\partial\widetilde{\alpha}\widetilde{v}_i}{\partial x_i}=0; \tag{8}$$
$$\frac{\partial\widetilde{\alpha}\widetilde{v}_i}{\partial t}+\frac{\partial\widetilde{\alpha}\widetilde{v_jv_i}}{\partial x_j}=\frac{1}{\tau_v}\widetilde{\alpha}(u_i-\widetilde{v}_i); \tag{9}$$
$$\frac{\partial\widetilde{\alpha}\widetilde{\vartheta}}{\partial t}+\frac{\partial\widetilde{\alpha}\widetilde{\vartheta v_i}}{\partial x_i}=\frac{1}{\tau_\vartheta}\widetilde{\alpha}(T-\widetilde{\vartheta}). \tag{10}$$

Single-point second-order correlation moments determine the kinetic energy of turbulence, the transfer of momentum and heat in the dispersed phase. Two-point second-order moments describe the spectrum of turbulence and the size of large-scale turbulent eddies, enabling to assess the correlation between fluctuations of various parameter values at unequally distant temporal and spatial points. Quadric moment equations have the following form

$$\frac{\partial\widetilde{\alpha}\widetilde{v_iv_j}}{\partial t}+\frac{\partial\widetilde{\alpha}\widetilde{v_iv_jv_k}}{\partial x_k}=\frac{1}{\tau_v}\widetilde{\alpha}(u_i\widetilde{v}_j+\widetilde{v}_iu_j-2\widetilde{v_iv_j}); \tag{11}$$
$$\frac{\partial\widetilde{\alpha}\widetilde{\vartheta v_i}}{\partial t}+\frac{\partial\widetilde{\alpha}\widetilde{\vartheta v_iv_k}}{\partial x_k}=\frac{1}{\tau_v}\widetilde{\alpha}(\widetilde{\vartheta}u_i-\widetilde{\vartheta v_j})+\frac{1}{\tau_\vartheta}\widetilde{\alpha}(T\widetilde{v}_i-\widetilde{\vartheta v_j}). \tag{12}$$

Single-point third-order moments describe the diffusion of turbulence, and two-point tertiary moments describe redistribution of energy over the turbulence spectrum.

2.3. Model closing. Components of the sub-grid stress tensor and components of the sub-grid heat flux vector look as follows

$$\sigma_{ij}=\widetilde{v_iv_j}-\widetilde{v}_i\widetilde{v}_j,\quad q_i=\widetilde{\vartheta v_i}-\widetilde{\vartheta}\widetilde{v}_i.$$

Averaging the dispersed phase parameters creates new terms of sum that require mathematical simulation. To complete equations (11) and (12), let's assume that the contribution of tertiary correlation moments is negligible [22]

$$\int(v-\widetilde{v}_i)(v-\widetilde{v}_j)(v-\widetilde{v}_k)\overline{W}(\boldsymbol{x},\boldsymbol{v},\vartheta,t)d\boldsymbol{v}d\vartheta=0;$$
$$\int(\vartheta-\widetilde{\vartheta})(v-\widetilde{v}_i)(v-\widetilde{v}_k)\overline{W}(\boldsymbol{x},\boldsymbol{v},\vartheta,t)d\boldsymbol{v}d\vartheta=0.$$

Using the approaches proposed in [22, 23] for calculating integrals, the equations for the tertiary moments are replaced by algebraic correlations

$$\widetilde{v_iv_jv_k}=\widetilde{v_jv_k}\widetilde{v}_i+\widetilde{v_iv_j}\widetilde{v}_k+\widetilde{v_iv_k}\widetilde{v}_j-2\widetilde{v}_i\widetilde{v}_j\widetilde{v}_k; \tag{13}$$
$$\widetilde{\vartheta v_iv_k}=\widetilde{\vartheta v_k}\widetilde{v}_i+\widetilde{\vartheta v_i}\widetilde{v}_k+\widetilde{v_iv_k}\widetilde{\vartheta}-2\widetilde{v}_i\widetilde{v}_k\widetilde{\vartheta}. \tag{14}$$

Ratios (13) and (14) provide a complete formulation of the problem.

The motion and heat transfer of the dispersed phase is described by equations (8)–(10) for the variables $\widetilde{\alpha}$, $\widetilde{v}_i$ and $\widetilde{\vartheta}$, and equations (11) and (12) for the variables $\widetilde{v_iv_j}$ and $\widetilde{\vartheta v_i}$.

By ignoring the inertial effects ($\tau_v = \tau_\vartheta = 0$), the speed and temperature of the dispersed phase are the same as the respective gas parameters ($\widetilde{v}_i = u_i$, $\widetilde{\vartheta} = T$). In this case, only equations for the numerical concentration of particles have to be solved, while the transfer equations (9)–(12) do not require solutions.

Partial consideration of inertial effects is possible with the equilibrium model, in which local velocity of the dispersed phase is expressed as a sum of the local velocity and acceleration of the gas medium. The dynamic and thermal relaxation time of a particle is used as a parameter in the expansion process. Assuming $\widetilde{v_iv_j} = \widetilde{v}_i\widetilde{v}_j$ and using equation (8), it can be inferred from equation (9) that the local acceleration of the dispersed phase equals local acceleration of the gas medium. The equilibrium model describes a number of inertial effects (preferential acceleration), but is only suitable for describing the motion of sufficiently small particles.

Complete accounting of inertial effects can be performed by solving the equations (8)–(11), assuming that the contribution of correlation moments described by equations (12) and (13) is negligible. In practice, it means that $\widetilde{v_iv_j} = \widetilde{v}_i\widetilde{v}_j$ and $\widetilde{\vartheta v_j} = \widetilde{\vartheta}\widetilde{v}_j$. In this case, the equations in the mathematical model appear to be equivalent to the model proposed in [30], which describes the gas suspension flows where particles occupy a negligibly small space and the ratio of dispersed phase to gaseous phase is sufficiently big. For gas suspension with monodispersed particles, the mathematical model equations are the same as those formulated in [**??**]. Despite taking into account the inertial effects, ignoring quadric correlation moments of the dispersed phase means omitting a number of important effects (crossing effect) that play an important role in the flow of a gas with suspended high-inertia particles.

3. Single-dimensional model. Let's consider equations describing the motion of inviscid compressible gas with particles in one-dimensional approximation. The effect of viscous forces is only taken into account on interaction between the gas and particles.

3.1. The gas. The equation describing an unsteady flow of inviscid compressible gas looks as follows in the conservative form

$$\frac{\partial \boldsymbol{Q}_g}{\partial t} + \frac{\partial \boldsymbol{F}_g}{\partial x} = \boldsymbol{S}_g. \tag{15}$$

The equation of state for an ideal gas, and the ratio for calculating specific total energy, are written as follows

$$p = \rho RT, \quad E = \frac{p}{\gamma - 1} + \frac{1}{2}\rho u^2.$$

The conservative variables vector $\boldsymbol{Q}_g$ and flux vector $\boldsymbol{F}_g$ have the form

$$\boldsymbol{Q}_g = \begin{pmatrix} \rho \\ \rho u \\ E \end{pmatrix}, \quad \boldsymbol{F}_g = \begin{pmatrix} \rho u \\ \rho u u + p \\ (E + p)u \end{pmatrix}.$$

Here, t is the time, x is the spatial coordinate, ρ is the density, u is the velocity in x direction, p is the pressure, T is the temperature, E is the total energy, R is the gas law constant, and γ is the ratio of specific heat capacities. The source term S_g takes into account the effect of the disperse phase. In dimensionless variables, it is assumed that $R = 1/\gamma$ and $\mu = 1/\mathrm{Re}$.

Equation (15) is written in linearized form as

$$\frac{\partial \boldsymbol{Q}_g}{\partial t} + A_g \frac{\partial \boldsymbol{Q}_g}{\partial x} = \boldsymbol{S}_g, \tag{16}$$

where $A_g = \partial \boldsymbol{F}_g / \partial \boldsymbol{Q}_g$ is the Jacobian. In physical variables, Jacobian has the form

$$A_g = \begin{pmatrix} 0 & 1 & 0 \\ \frac{1}{2}(\gamma - 3)u^2 & (3 - \gamma)u & \gamma - 1 \\ \frac{1}{2}(\gamma - 1)u^3 - uH & H - (\gamma - 1)u^2 & \gamma u \end{pmatrix},$$

where $H = (E + p)/\rho$ is the specific total enthalpy. Jacobian is represented in the form $A_g = R_g \Lambda_g L_g$, where Λ_g is a diagonal matrix with Jacobian eigenvalues along the main diagonal, and L_g and R_g are matrices consisting

of left and right Jacobian eigenvectors, and $L_g = R_g^{-1}$. The Jacobian has three real eigenvalues

$$\lambda_1 = u - c, \quad \lambda_2 = u, \quad \lambda_3 = u + c,$$

where c is the speed of sound. The speed of sound is found from the ratio

$$c = \left[(\gamma - 1)\left(H - \frac{1}{2}u^2\right)\right]^{1/2}.$$

The right Jacobian eigenvectors have the form

$$r_1 = \begin{pmatrix} 1 \\ u - c \\ H - uc \end{pmatrix}, \quad r_2 = \begin{pmatrix} 1 \\ u \\ \frac{1}{2}u^2 \end{pmatrix}, \quad r_3 = \begin{pmatrix} 1 \\ u + c \\ H + uc \end{pmatrix}.$$

Variables corresponding to the zero component of i-th eigenvector do not change when crossing the i characteristic. Expressions for right eigenvectors are used when constructing flow limiters in high resolution schemes.

Diagonalization of the Jacobian allows one to rewrite equation (16) in the characteristic form

$$\frac{\partial \boldsymbol{W}_g}{\partial t} + \Lambda_g \frac{\partial \boldsymbol{W}_g}{\partial x} = \boldsymbol{S}_g, \tag{17}$$

where $\boldsymbol{W}_g = R_g^{-1}\boldsymbol{Q}_g$ represents a characteristic variables vector.

3.2. Dispersed phase. The equation describing the motion and heat exchange in the dispersed phase is written in the conservative form as

$$\frac{\partial \boldsymbol{Q}_p}{\partial t} + \frac{\partial \boldsymbol{F}_p}{\partial x} = \boldsymbol{S}_p. \tag{18}$$

The conservative variables vector $\boldsymbol{Q}_p$ and the flux vector $\boldsymbol{F}_p$ have the following forms

$$\boldsymbol{Q}_p = \begin{pmatrix} \widetilde{\alpha} \\ \widetilde{\alpha}\widetilde{v} \\ \widetilde{\alpha}\widetilde{\vartheta} \\ \widetilde{\alpha}\widetilde{v}\widetilde{v} \\ \widetilde{\alpha}\widetilde{v}\widetilde{\vartheta} \end{pmatrix}, \quad \boldsymbol{F}_p = \begin{pmatrix} \widetilde{\alpha}\widetilde{v} \\ \widetilde{\alpha}\widetilde{v}\widetilde{v} \\ \widetilde{\alpha}\widetilde{\vartheta}\widetilde{v} \\ \widetilde{\alpha}(3\widetilde{v}\widetilde{v}\widetilde{v} - 2\widetilde{v}^3) \\ \widetilde{\alpha}(2\widetilde{\vartheta}\widetilde{v}\widetilde{v} + \widetilde{\vartheta}\widetilde{v}\widetilde{v} - 2\widetilde{\vartheta}\widetilde{v}\widetilde{v}) \end{pmatrix}.$$

The source term accounting for the interphase motion and heat transfer is

$$\boldsymbol{S}_p = \begin{pmatrix} 0 \\ \widetilde{\alpha}(u - \widetilde{v})/\tau_v \\ \widetilde{\alpha}(T - \widetilde{\vartheta})/\tau_\vartheta \\ 2\widetilde{\alpha}(u\widetilde{v} - \widetilde{v}\widetilde{v})/\tau_v \\ \widetilde{\alpha}(\widetilde{\vartheta}u - \widetilde{\vartheta}\widetilde{v})/\tau_v + \widetilde{\alpha}(T\widetilde{v} - \widetilde{\vartheta}\widetilde{v})/\tau_\vartheta \end{pmatrix}.$$

The source term accounting for the interphase motion and heat transfer in equation (15) is

$$\boldsymbol{S}_g = \begin{pmatrix} 0 \\ m_p\widetilde{\alpha}(\widetilde{v} - u)/\tau_v \\ \beta m_p\widetilde{\alpha}(\widetilde{\vartheta} - T)/\tau_\vartheta + m_p\widetilde{\alpha}(\widetilde{v}\widetilde{v} - u\widetilde{v})/\tau_v \end{pmatrix}.$$

Equation (18) describing the motion and heat transfer in the dispersed phase, is of hyperbolic nature. In quasi-linear form, equation (18) takes the form

$$\frac{\partial \boldsymbol{Q}_p}{\partial t} + A_p \frac{\partial \boldsymbol{Q}_p}{\partial x} = \boldsymbol{S}_p, \tag{19}$$

where $A_p = \partial \boldsymbol{F}_p / \partial \boldsymbol{Q}_p$ is the Jacobian. Jacobian looks as follows

$$A_p = \begin{pmatrix} 0 & 1 & 0 & 0 & 0 \\ 0 & 0 & 0 & 1 & 0 \\ 0 & 0 & 0 & 0 & 1 \\ -3\widetilde{v}\widetilde{v}\widetilde{v} + 4\widetilde{v}^3 & 3\widetilde{v}\widetilde{v} - 6\widetilde{v}^2 & 0 & 3\widetilde{v} & 0 \\ -\widetilde{\vartheta}\widetilde{v}\widetilde{v} - 2\widetilde{\vartheta}\widetilde{v}\widetilde{v} + 4\widetilde{\vartheta}\widetilde{v}\widetilde{v} & 2\widetilde{\vartheta}\widetilde{v} - 4\widetilde{\vartheta}\widetilde{v} & \widetilde{v}\widetilde{v} - 2\widetilde{v}^2 & \widetilde{\vartheta} & 2\widetilde{v} \end{pmatrix}.$$

Jacobian is represented in the form $A_p = R_p \Lambda_p L_p$, where Λ_p is a diagonal matrix with Jacobian eigenvalues along the main diagonal, and L_p and R_p are matrices consisting of left and right Jacobian eigenvectors, and $L_p = R_p^{-1}$. Jacobian has five real eigenvalues

$$\lambda_1 = \widetilde{v}, \quad \lambda_2 = \widetilde{v} + \sqrt{3}\sigma, \quad \lambda_3 = \widetilde{v} - \sqrt{3}\sigma, \quad \lambda_4 = \widetilde{v} + \sigma, \quad \lambda_5 = \widetilde{v} - \sigma,$$

where

$$\sigma = (\widetilde{v\upsilon} - \widetilde{v}\widetilde{\upsilon})^{1/2}.$$

Given a non-negative kernel $H_\Delta(\boldsymbol{x})$, σ is a real number [26, 28], and this guarantees hyperbolicity of equation (19). The right Jacobian eigenvectors have the form

$$r_1 = \begin{pmatrix} 1 \\ \lambda_1 \\ \widetilde{\vartheta} \\ \lambda_1^2 \\ \lambda_1 \widetilde{\vartheta} \end{pmatrix}, \quad r_2 = \begin{pmatrix} 1 \\ \lambda_2 \\ \chi_2 \\ \lambda_2^2 \\ \lambda_2 \chi_2 \end{pmatrix}, \quad r_3 = \begin{pmatrix} 1 \\ \lambda_3 \\ \chi_3 \\ \lambda_3^2 \\ \lambda_3 \chi_3 \end{pmatrix}, \quad r_4 = \begin{pmatrix} 0 \\ 0 \\ 1 \\ 0 \\ \lambda_4 \end{pmatrix}, \quad r_5 = \begin{pmatrix} 0 \\ 0 \\ 1 \\ 0 \\ \lambda_5 \end{pmatrix}.$$

Here

$$\chi_2 = \lambda_2 \frac{(3\lambda_2 \widetilde{v\upsilon} - 9\widetilde{v\upsilon}\widetilde{\upsilon} + 8\widetilde{v}^3 - 2\lambda_2 \widetilde{v}^2)(\lambda_2 \widetilde{\vartheta} - 4\widetilde{\vartheta}\widetilde{\upsilon} + 3\widetilde{\vartheta v})}{3(\lambda_2 \widetilde{v\upsilon} - \lambda_2 \widetilde{v}^2 - 2\widetilde{v\upsilon}\widetilde{\upsilon} + 2\widetilde{v}^3)(3\widetilde{v\upsilon} - 4\widetilde{v}^2)};$$
$$\chi_3 = \lambda_3 \frac{(3\lambda_3 \widetilde{v\upsilon} - 9\widetilde{v\upsilon}\widetilde{\upsilon} + 8\widetilde{v}^3 - 2\lambda_3 \widetilde{v}^2)(\lambda_3 \widetilde{\vartheta} - 4\widetilde{\vartheta}\widetilde{\upsilon} + 3\widetilde{\vartheta v})}{3(\lambda_3 \widetilde{v\upsilon} - \lambda_3 \widetilde{v}^2 - 2\widetilde{v\upsilon}\widetilde{\upsilon} + 2\widetilde{v}^3)(3\widetilde{v\upsilon} - 4\widetilde{v}^2)}.$$

Diagonalization of the Jacobian allows one to rewrite equation (19) in the characteristic form

$$\frac{\partial \boldsymbol{W}_p}{\partial t} + \Lambda_p \frac{\partial \boldsymbol{W}_p}{\partial x} = \boldsymbol{S}_p, \tag{20}$$

where $\boldsymbol{W}_p = R_p^{-1} \boldsymbol{Q}_p$ represents a characteristic variables vector.

4. Numerical method. The finite volume method is used for discretization of the governing equations, and the Godunov method is used to calculate fluxes across the boundaries of control volumes [33]. The Runge–Kutta third order method is used for integration over time.

Let's consider a uniform mesh consisting of N cells with the cell centers located in points $x_i = i\Delta x$, where $i = 0, 1, \ldots, N$. The conservative variables vector averaged over cell $[x_{i-1/2}, x_{i+1/2}]$ is determined by ratio

$$\boldsymbol{Q}_i = \frac{1}{\Delta x_i} \int\limits_{x_{i-1/2}}^{x_{i+1/2}} \boldsymbol{Q} dx,$$

where $\Delta x = x_{i+1/2} - x_{i-1/2}$. In discrete form, with layer n over time, equation (15) is written as follows

$$\boldsymbol{Q}_i^{n+1} = \boldsymbol{Q}_i^n - \frac{\Delta t}{\Delta x} \left(\boldsymbol{F}_{i+1/2}^n - \boldsymbol{F}_{i-1/2}^n \right). \tag{21}$$

The flows are found from the ratios

$$\boldsymbol{F}_{i-1/2}^n = \widetilde{\boldsymbol{F}}(\boldsymbol{Q}_{i-1}^n, \boldsymbol{Q}_i^n), \quad \boldsymbol{F}_{i+1/2}^n = \widetilde{\boldsymbol{F}}(\boldsymbol{Q}_i^n, \boldsymbol{Q}_{i+1}^n).$$

The tilde corresponds to numerical flow. The integration interval by time is chosen based on the condition

$$\Delta t = \mathrm{CFL} \frac{\Delta x}{\max\{|\lambda_i|\}},$$

where the number of Courant–Friedrichs–Lewy CFL $\leqslant 1/2$.

Using flux vector splitting, the Jacobian is represented as $A = R(\Lambda^+ + \Lambda^-)R^{-1}$, $A^+ = R\Lambda^+R^{-1}$, $A^- = R\Lambda^-R^{-1}$, where matrices Λ^+ and Λ^- are diagonal matrices with positive and negative eigenvalues on the main diagonal. Equation (21) takes the form

$$\boldsymbol{Q}_i^{n+1} = \boldsymbol{Q}_i^n - \frac{\Delta t}{\Delta x}\left(A^+\Delta\boldsymbol{Q}_{i-1/2} + A^-\Delta\boldsymbol{Q}_{i+1/2}\right). \tag{22}$$

Here

$$A^+\Delta\boldsymbol{Q}_{i-1/2} = R\Lambda^+R^{-1}(\boldsymbol{Q}_i - \boldsymbol{Q}_{i-1})A^-\Delta\boldsymbol{Q}_{i+1/2} = R\Lambda^-R^{-1}(\boldsymbol{Q}_{i+1} - \boldsymbol{Q}_i) = A\boldsymbol{Q}_i - \boldsymbol{F}_{i-1/2}^n;$$
$$A^-\Delta\boldsymbol{Q}_{i+1/2} = R\Lambda^-R^{-1}(\boldsymbol{Q}_{i+1} - \boldsymbol{Q}_i)A^+\Delta\boldsymbol{Q}_{i-1/2} = R\Lambda^-R^{-1}(\boldsymbol{Q}_1 - \boldsymbol{Q}_{i-1}) = -A\boldsymbol{Q}_i + \boldsymbol{F}_{i+1/2}^n.$$

The difference scheme (23) takes the form

$$\boldsymbol{Q}_i^{n+1} = \boldsymbol{Q}_i^n - \frac{\Delta t}{\Delta x}\left(\widehat{A}^+_{i-1/2}\Delta\boldsymbol{Q}_{i-1/2} + \widehat{A}^-_{i+1/2}\Delta\boldsymbol{Q}_{i+1/2}\right). \tag{23}$$

In the difference scheme (23), the components of A^+ and A^- matrices are located using Roe-averaged values.

For the gas phase, Roe averaging is set by the following ratios

$$\widehat{u}_{i-1/2} = \frac{\rho_{i-1}^{1/2}u_{i-1} + \rho_i^{1/2}u_i}{\rho_{i-1}^{1/2} + \rho_i^{1/2}};$$
$$\widehat{H}_{i-1/2} = \frac{\rho_{i-1}^{1/2}H_{i-1} + \rho_i^{1/2}H_i}{\rho_{i-1}^{1/2} + \rho_i^{1/2}} = \frac{(E_{i-1} + p_{i-1})/\rho_{i-1}^{1/2} + (E_i + p_i)/\rho_i^{1/2}}{\rho_{i-1}^{1/2} + \rho_i^{1/2}}.$$

The speed of sound is found from the ratio

$$\widehat{c} = \left[(\gamma - 1)\left(\widehat{H} - \frac{1}{2}\widehat{u}^2\right)\right]^{1/2}.$$

For the dispersed phase, averaging is set by the following ratios

$$\widehat{q}_{i-1/2} = \frac{1}{2}\left(q_{i-1} + q_i\right),$$

where q is a generalized variable ($q = \widetilde{v}$, $\widetilde{\vartheta}$, $\widetilde{vv}$, $\widetilde{\vartheta v}$).

5. Computation results. Let's consider the interaction of a steady-state subsonic and supersonic flow of inviscid compressible gas with a layer of particles that fill a limited space and are stationary at the initial moment in time.

5.1. Configuration of the computational region. Let's consider a uniform layer of spherically shaped solid particles blocking the cross-section of the channel which a uniform flow or a flat shock wave flows through (Figure 1).

A two-phase flow is computed and the dynamics of the particle layer behind the shock wave are investigated. Calculations are made at the interval of $[-5, 6]$. The particle layer consists of $8.6 \cdot 10^4$ particles, which are stationary at the initial moment in time, evenly filling the $0 \leqslant x \leqslant 0.3$ interval. The computational mesh contains 1000 points, of which about 100 belong to the particle layer.

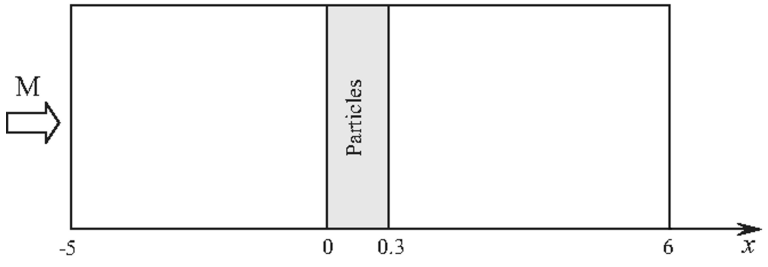

Figure 1. Flow interaction with the particles layer

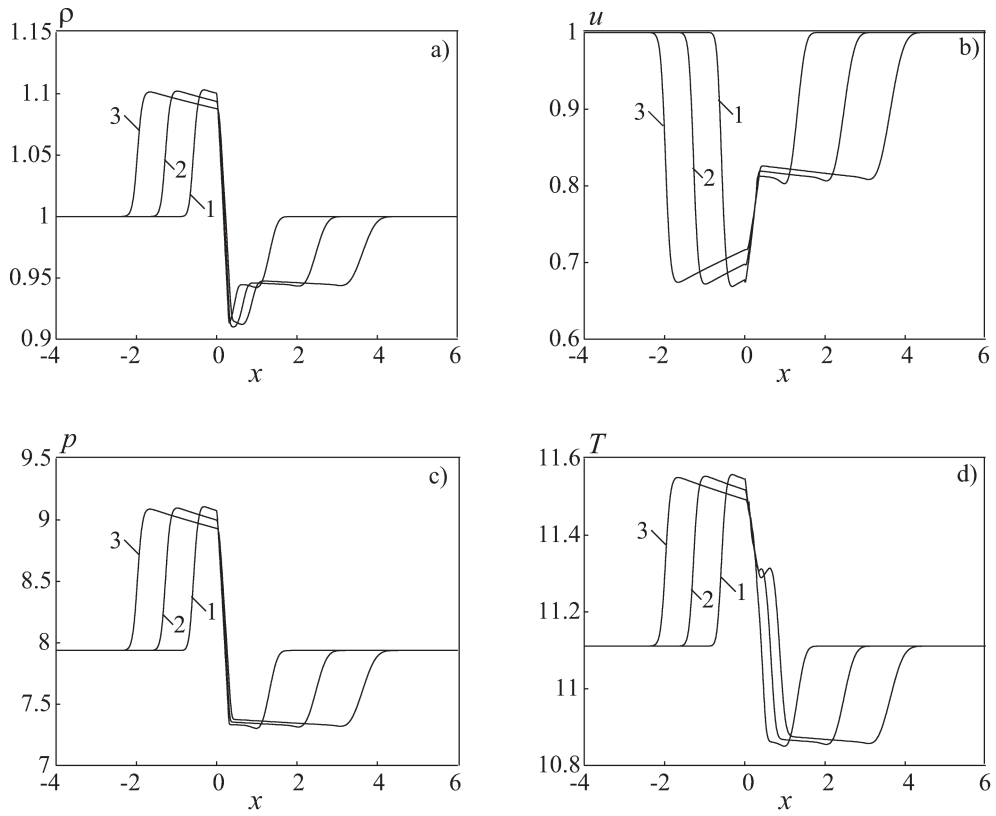

Figure 2. Density (a), velocity (b), pressure (c) and temperature (d) distributions of the gas phase in Case 1 at times $t = 0.275$ (1); 0.550 (2); 0.825 (3)

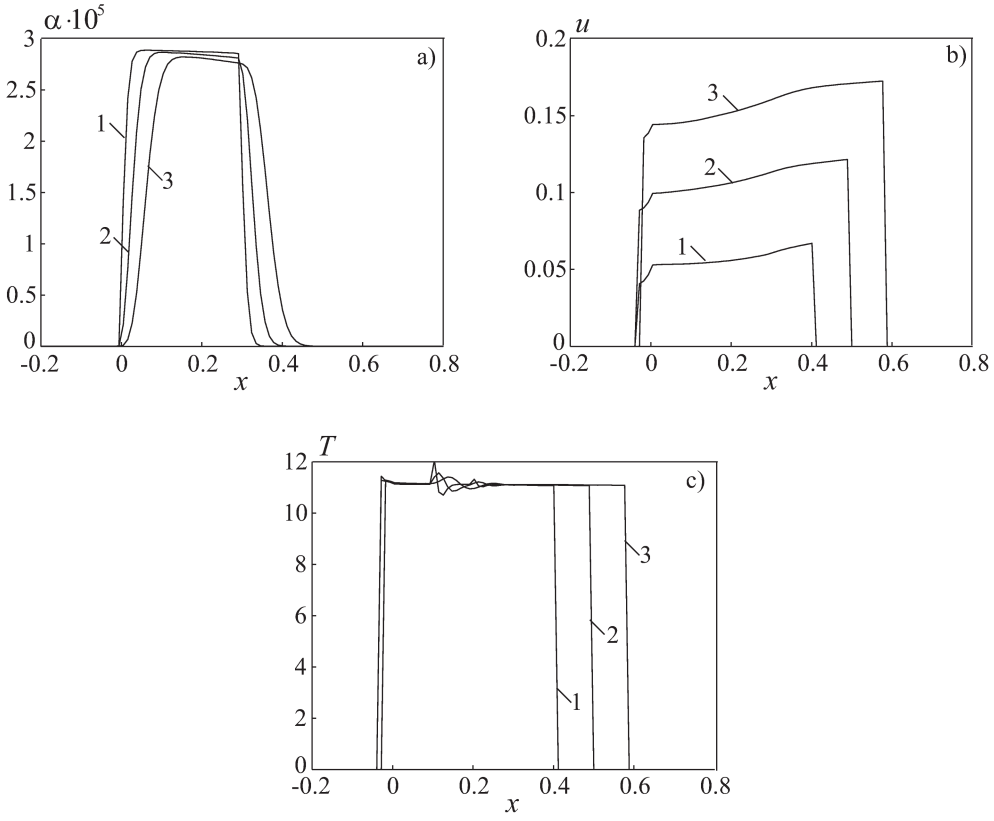

Figure 3. Density (a), velocity (b) and temperature (c) distributions of the dispersed phase in Case 1 at times $t = 0.275$ (1); 0.550 (2); 0.825 (3)

Air is chosen as the working medium. The ratio of specific heat capacities at constant pressure and constant volume is $\gamma = 1.4$. Kinematic viscosity and the Prandtl number are assigned the following values $\nu = 1.57 \cdot 10^{-5}$ m^2/s and Pr = 0.72. The ratio of material particle heat capacity to the gas heat capacity at constant pressure is assumed to be $\beta = 1$. In practice, the dynamic relaxation and thermal relaxation times turn out close to one another. It is assumed during the calculations that $\tau_v = \tau_\vartheta = 3.569$ s (in dimensionless variables, the relaxation time corresponds to the Stokes number). Particle material density and particle mass equal $\rho_p = 1000$ kg/m^3 and $m_p = 1.0055 \cdot 10^{-4}$ kg respectively (particle diameter $d_p = 5.77 \cdot 10^{-3}$ m).

On the left boundary, which is where working gas enters the computational domain, the Mach number is set to 0.3 in the case of a subsonic flow (Case 1). In the case of a supersonic flow (Case 2), the left boundary parameters are derived from the Rankine–Hugoniot relationships, so that Mach number behind the pressure front equals 2.8. Free outflow conditions are used at the output boundary.

At the initial moment $t = 0$, the gas flows at a uniform velocity ($\rho = 1$, $p = 1$ and $u = 1$ in dimensionless variables). Particle velocity is set at zero, and the particle temperature is assumed to be the same as the gas temperature. The correlation moments of speed and temperature of the dispersed phase are zero ($\widetilde{v} = 0$, $\widetilde{\vartheta} = T_g$, $\widetilde{vv} = 0$, $\widetilde{\vartheta v} = 0$). Numerical concentration of the dispersed phase is $2.885 \cdot 10^5$ m^{-3}. Particles of different sizes have different inertia rates and different speed and temperature lags in relation to the gas flow, which affects the establishment of a quasi-stationary flow.

To validate the developed computational algorithm, a number of model tasks in unsteady one-dimensional gas dynamics are solved. The various tasks are established in [34]. In this case, vanishingly small values (around 10^{-8} m^{-3}) are used for the initial concentration of the dispersed phase.

5.2. Subsonic flow. The distributions of carrier gas parameters at different moments in time are shown in Figure 2. The flow slows down in front of the particle layer, which results in a reduced speed and increase in gas density, pressure and temperature. When the incoming flow encounters the particle layer, the particles that are at rest at the initial point in time begin to accelerate, acquiring a non-zero speed and reducing resistance to the gas flow, which leads to an increase in the carrier flow velocity. Behind the area occupied by the particles, the flow density, velocity, pressure and temperature are restored to the corresponding values in the incoming flow.

The distributions of dispersed phase parameters at different points in time are shown in Figure 3, and the distribution of correlation moments of the dispersed phase is presented in Figure 4. At time $t = 0.275$ there is no noticeable displacement of the particle layer, although the dispersed phase density at the left boundary of the layer is slightly higher than at its right boundary. Within the area occupied by the particles, the speed of the dispersed phase is distributed unevenly. Near the right boundary of the layer, the speed of the dispersed phase increases as the carrier gas accelerates in this area. Particles located near the left boundary of the layer have the highest velocity, as their interaction with the gas flow begins at the moment the gas reaches the area occupied by the particles. The temperature of the dispersed phase remains more or less constant. Uneven velocity distribution along the particle layer (higher at the left boundary and lower at the right boundary) results in different heat transfer rates between the gas and particles located near the left and right boundary of the layer. This results in a slight decrease in temperature of the dispersed phase near the right boundary of the layer. Distributions of the correlation moments of velocity and velocity-temperature of the dispersed phase are qualitatively similar.

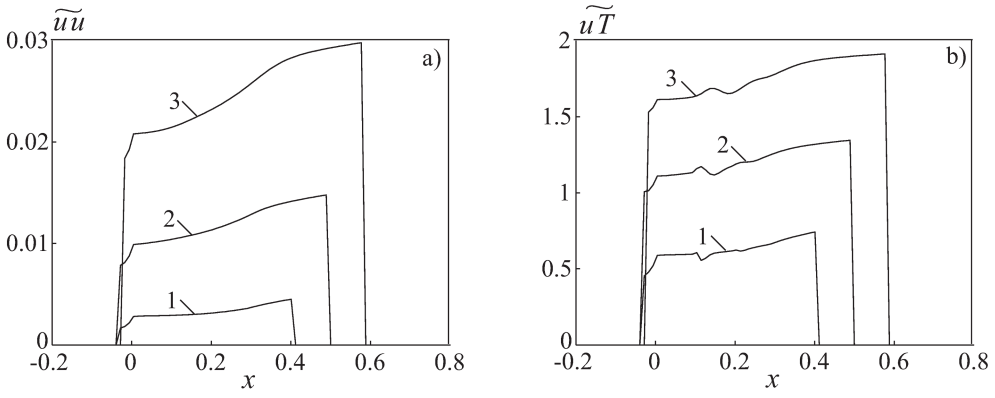

Figure 4. Distributions of the correlation moment of velocity (a) and the correlation moment of velocity and temperature (b) of the dispersed phase in Case 1 at time $t = 0.275$ (1); 0.550 (2); 0.825 (3)

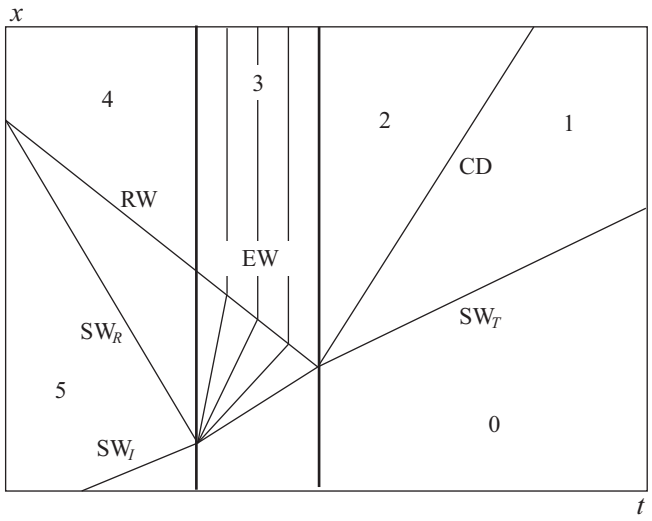

Figure 5. Shock wave interaction with a particle cloud (SW_I is the incoming shock wave, SW_R is the reflected shock wave, SW_T is the transmitted shock wave, CD is the contact discontinuity, RW is the rarefaction wave, EW is the expansion wave fan)

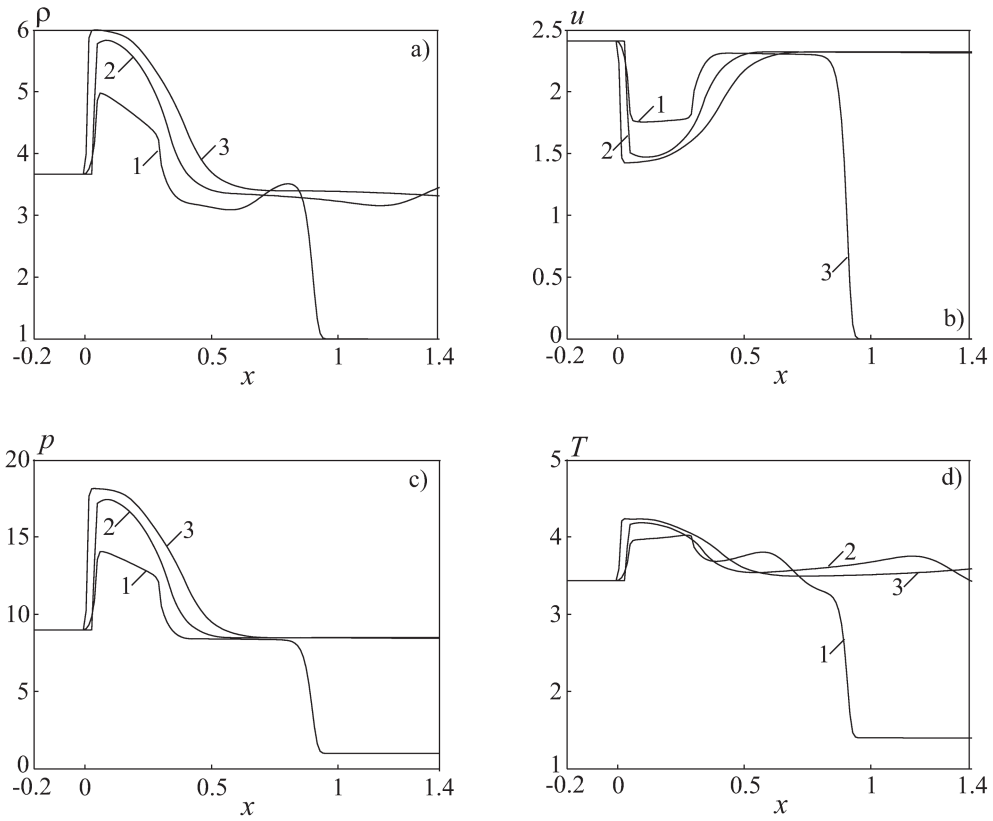

Figure 6. Density (a), velocity (b), pressure (c) and temperature (d) distributions of the gas phase in Case 2 at times $t = 0.275$ (1); 0.550 (2); 0.825 (3)

5.3. Supersonic flow. Based on the analysis of (x, t) diagram shown in Figure 5 (particles are considered to be frozen in space), which was produced as a result of computations, the interaction between the shock wave and the particle layer can be described as follows [35]. When the incoming shock wave SW_I reaches the left boundary of the particle layer and starts penetrating it, a reflected shock wave SW_R is formed, which spreads in the opposite direction of the incoming shock wave, and a transmitted shock wave SW_T, which moves in the same direction as the incoming shock wave. The transmitted shock wave is followed by the expansion wave fan

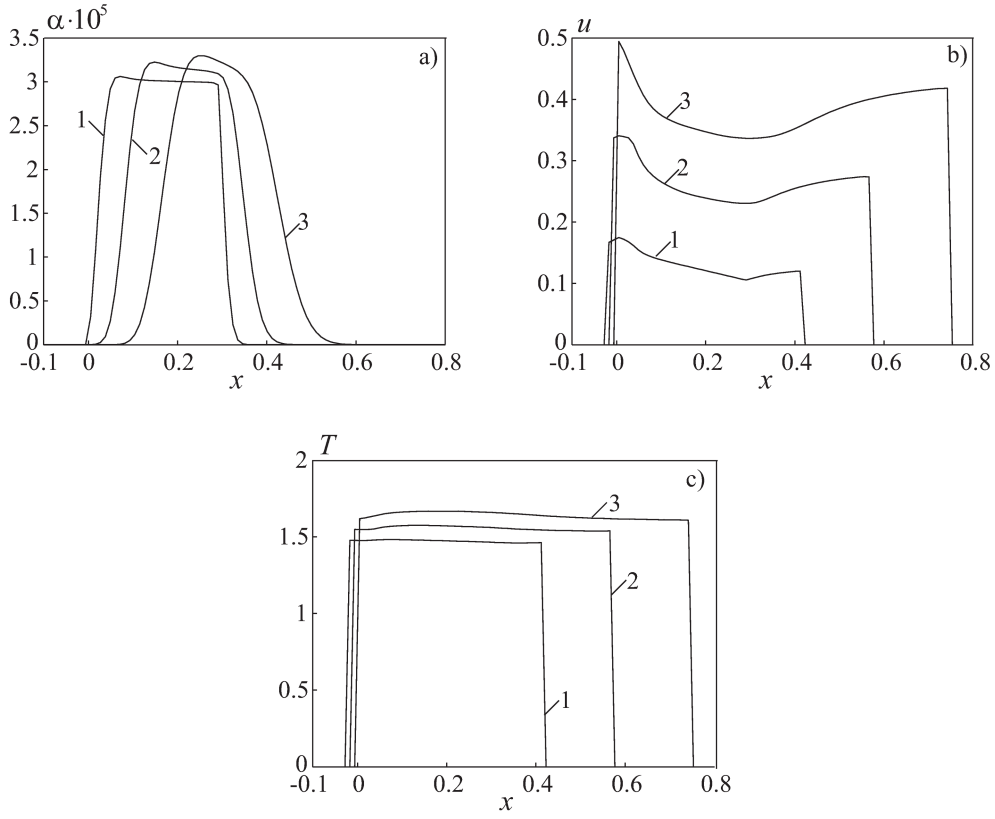

Figure 7. Density (a), velocity (b) and temperature (c) distributions of the dispersed phase in Case 2 at times $t = 0.275$ (1); 0.550 (2); 0.825 (3)

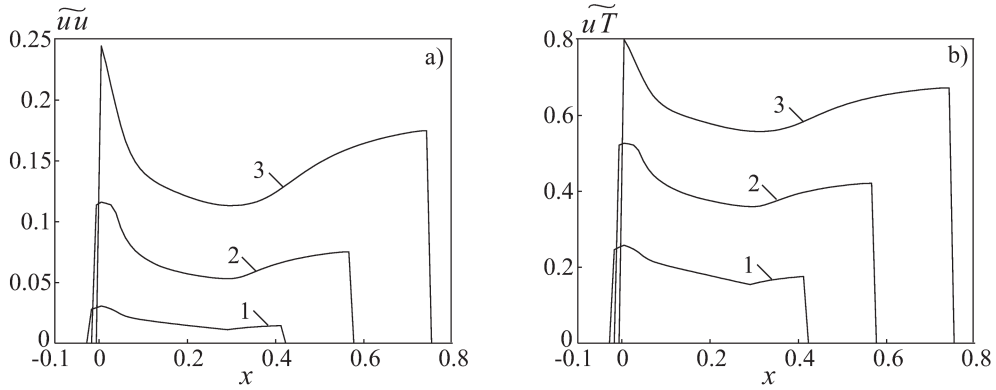

Figure 8. Distributions of the correlation moment of velocity (a) and the correlation moment of velocity and temperature (b) of the dispersed phase in Case 2 at times $t = 0.275$ (1); 0.550 (2); 0.825 (3)

EW inside the layer (negative pressure gradient), in which the gas is accelerated, so the flow reaches supersonic speed near the right boundary of the particle layer. When the transmitted shock wave exits the particle layer, another rarefaction wave fan RW is formed, and a contact discontinuity CD exits the layer together with the transmitted shock wave, which separates the transmitted shock wave from the rarefaction waves. Interaction between the expansion wave fan EW and the rarefaction wave RW results in the establishment of a constant pressure gradient in the particle layer. The intensity of the transmitted shock wave decreases compared to the incoming shock wave, as some of the gas energy is spent on accelerating the particles. Over time, a constant pressure gradient is established in the particle layer.

The calculations performed allow identification of six characteristic flow areas (Figure 5: 0 — undisturbed gas area; 1 — area corresponding to the gas behind the transmitted shock wave SW_T; 2 — area corresponding to the gas between contact discontinuity CD and the right edge of the particle layer; 3 — area occupied by the expansion wave fan EW; 4 — area corresponding to the gas behind the reflected shock wave SW_R; 5 — area corresponding to the conditions at the front of the incoming shock wave SW_I.

The distributions of carrier gas parameters at different moments in time are shown in Figure 6. The interaction of supersonic gas flow with the particle layer results in the formation of a shock wave, which is followed by a sudden decrease in gas velocity to subsonic values and an increase in its density, pressure and temperature. Behind the shock wave front, the carrier flow interacts with the particles. In the area occupied by the particles, the carrier flow rate remains approximately constant while the gas density, pressure and temperature decrease. Particles that are at rest at the initial moment in time get entrained by the gas flow, gaining a non-zero speed and providing less resistance to the gas flow. At the right boundary of the particle layer, a rarefaction wave is observed, where the gas flow velocity increases and density, pressure and temperature decrease. Behind the particle layer, the gas parameters never reach the values they had in the undisturbed flow, which is caused by non-isentropic energy losses at the shock wave front. Behind the rarefaction wave fan, the gas velocity and pressure are lower than in the undisturbed flow. The density and temperature behind the expansion wave fan experience minor fluctuations as a result of contact discontinuity, which moves downstream at a speed lower than that of the shock wave induced by the particle layer. To the left of the contact discontinuity, the gas temperature is higher and its density is lower than the temperature and density of the gas to the right of the contact discontinuity. The contact discontinuity occurs as a result of a sudden change in gas density and temperature at the shock wave front moving downstream.

Comparison of gas parameter distributions at different points in time shows that the position of the shock wave front induced by the particle layer remains virtually unchanged in space, but the magnitude of the flow parameter fluctuations increases over time.

The distributions of dispersed phase parameters at different points in time are shown in Figure 7, and the distribution of correlation moments of the dispersed phase are presented in Figure 8. At time $t = 0.275$, the particle velocity near the left boundary of the layer exceeds the velocity of the particles near its right boundary. Uneven velocity distribution results in uneven density distribution in the dispersed phase, which is much higher at the left boundary of the layer than on its right boundary. An increase in the gas temperature at the left boundary of the layer leads to an increase in the temperature of the dispersed phase. Distributions of the correlation moments of velocity and velocity-temperature of the dispersed phase are qualitatively similar.

6. Conclusion. A mathematical model describing unsteady flow of gas with inert particles is constructed within the model of interpenetrating continuums. The gas and dispersed phases are described by sets of equations expressing the laws of mass, momentum and energy conservation, while interactions between the phases are taken into account using source terms. Hyperbolic equations are used to describe the gas and dispersed phases, allowing the recording in conservative form, which means Godunov type methods can be used to find numerical solutions.

Numerical simulation of flow interaction at subsonic and supersonic speeds is performed, with a layer of particles being stationary at the initial point in time. Shock-wave flow structure and space-time dependencies of particle concentration and other flow parameters are shown. The results obtained allow estimating the shock wave attenuation caused by interaction with the dispersed phase.

The research was carried out with the financial support of the Russian Science Foundation (project No. 19–71–10019).

References

1. K. N. Volkov and V. N. Emelyanov, Flows of Gas with Particles (Fizmatlit, Moscow, 2008) [in Russian].

2. Kh. A. Rakhmatulin, Fundamentals of the Gasdynamics of Interpenetrating Motions of Continuous Media, Prikl. Mat. Mekh. 20 (2), 184–195 (1956).

3. A. N. Kraiko and L. E. Sternin, Theory of Flows of a Two-Velocity Continuous Medium Containing Solid or Liquid Particles, Prikl. Mat. Mekh. 29 (3), 418–429 (1965) [J. Appl. Math. Mech. 29 (3), 482–496 (1965)].

4. H. Staedtke, G. Franchello, B. Worth, et al., Advanced Three-Dimensional Two-Phase Flow Simulation Tools for Application to Reactor Safety (ASTAR), Nucl. Eng. Des. 235 (2–4), 379–400 (2005).

5. R. I. Nigmatulin, Dynamics of Multiphase Media (Nauka, Moscow, 1987; Hemisphere, New York, 1990).

6. A. N. Kraiko, On Correctness of the Cauchy Problem for a Two-Fluid Model of a Gas Flow Containing Particles, Prikl. Mat. Mekh. 46 (3), 420–428 (1982) [J. Appl. Math. Mech. 46 (3), 327–333 (1982)].

7. A. N. Osiptsov, Investigation of Regions of Unbounded Growth of the Particle Concentration in Disperse Flows, Izv. Akad. Nauk SSSR, Mekh. Zhidk. Gaza, No. 3, 46–52 (1984) [Fluid Dyn. 19 (3), 378–385 (1984)].

8. M. R. Baer and J. W. Nunziato, A Two-Phase Mixture Theory for the Deflagration-to-Detonation Transition (DDT) in Reactive Granular Materials, Int. J. Multiph. Flow 12 (6), 861–889 (1986).

9. Y.-Y. Niu, Numerical Approximations of a Compressible Two Fluid Model by the Advection Upwind Splitting Method, Int. J. Numer. Methods Fluids 36 (3), 351–371 (2001).

10. P. Embid and M. Baer, Mathematical Analysis of a Two-Phase ContinuumMixture Theory, Continuum Mech. Therm. 4, 279–312 (1992).

11. E. F. Toro, Riemann-Problem-Based Techniques for Computing Reactive Two-Phase Flows, in Lecture Notes in Physics (Springer, Heidelberg, 1989), Vol. 351, pp. 472–481.

12. I. Toumi, An Upwind Numerical Method for Two-Fluid Two-Phase Flow Models, Nucl. Sci. Eng. 123 (2), 147–168 (1996).

13. C.-H. Chang and M.-S. Liou, A Robust and Accurate Approach to Computing Compressible Multiphase Flow: Stratified Flow Model and AUSM$^+$-up Scheme, J. Comput. Phys. 225 (1), 840–873 (2007).

14. N. Andrianov and G. Warnecke, The Riemann Problem for the Baer–Nunziato Model of Two-Phase Flows, J. Comput. Phys. 195 (2), 434–464 (2004).

15. D. W. Schwendeman, C. W. Wahle, and A. K. Kapila, The Riemann Problem and a High-Resolution Godunov Method for a Model of Compressible Two-Phase Flow, J. Comput. Phys. 212 (2), 490–526 (2006).

16. V. Deledicque and M. V. Papalexandris, An Exact Riemann Solver for Compressible Two-Phase Flow Models Containing Non-conservative Products, J. Comput. Phys. 222 (1), 217–245 (2007).

17. S. Karni and G. Hernandez-Duenas, A Hybrid Algorithm for the Baer–Nunziato Model Using the Riemann Invariants, J. Sci. Comput. 45, 382–403 (2010).

18. C. A. Lowe, Two-Phase Shock-Tube Problems and Numerical Methods of Solution, J. Comput. Phys. 204 (2), 598–632 (2005).

19. C. Pares, Numerical Methods for Nonconservative Hyperbolic Systems: A Theoretical Framework, SIAM J. Numer. Anal. 44 (1), 300–321 (2006).

20. S. Rhebergen, O. Bokhove, and J. J. W. van der Vegt, Discontinuous Galerkin Finite Element Methods for Hyperbolic Nonconservative Partial Differential Equations, J. Comput. Phys. 227 (3), 1887–1922 (2008).

21. S. A. Tokareva and E. F. Toro, HLLC-Type Riemann Solver for the Baer–Nunziato Equations of Compressible Two-Phase Flow, J. Comput. Phys. 229 (10), 3573–3604 (2010).

22. R. V. R. Pandya and F. Mashayek, Two-Fluid Large-Eddy Simulation Approach for Particle-Laden Turbulent Flows, Int. J. Heat Mass Tran. 45 (24), 4753–4759 (2002).

23. B. Shotorban, Preliminary Assessment of Two-Fluid Model for Direct Numerical Simulation of Particle-Laden Flows, AIAA J. 49 (2), 438–443 (2011).

24. L. I. Zaichik, O. Simonin, and V. M. Alipchenkov, An Eulerian Approach for Large Eddy Simulation of Particle Transport in Turbulent Flows, J. Turbul. 10 (9), 1–21 (2009).

25. B. Shotorban and S. Balachandar, Two-Fluid Approach for Direct Numerical Simulation of Particle-Laden Turbulent Flows at Small Stokes Numbers, Phys. Rev. E 79 (2009).
doi 10.1103/PhysRevE.79.056703

26. B. Shotorban, G. B. Jacobs, O. Ortiz, and Q. Truong, An Eulerian Model for Particles Nonisothermally Carried by a Compressible Fluid, Int. J. Heat Mass Tran. 65, 845–854 (2013).

27. F. Mashayek and R. V. R. Pandya, Analytical Description of Particle/Droplet-Laden Turbulent Flows, Prog. Energy Combust. Sci. 29 (4), 329–378 (2003).

28. B. Vreman, B. Geurts, and H. Kuerten, Realizability Conditions for the Turbulent Stress Tensor in Large-Eddy Simulation, J. Fluid Mech. 278, 351–362 (1994).

29. L. Y. M. Gicquel, P. Givi, F. A. Jaberi, and S. B. Pope, Velocity Filtered Density Function for Large Eddy Simulation of Turbulent Flows, Phys. Fluids 14 (3), 1196–1213 (2002).

30. T. Saito, Numerical Analysis of Dusty-Gas Flows, J. Comput. Phys. 176 (1), 129–144 (2002).

31. F. Laurent, M. Massot, and P. Villedieu, Eulerian Multi-Fluid Modeling for the Numerical Simulation of Coalescence in Polydisperse Dense Liquid Sprays, J. Comput. Phys. 194 (2), 505–543 (2004).

32. D. Kah, F. Laurent, M. Massot, and S. Jay, A High Order Moment Method Simulating Evaporation and Advection of a Polydisperse Liquid Spray, J. Comput. Phys. 231 (2), 394–422 (2012).

33. R. J. LeVeque, Finite Volume Methods for Hyperbolic Problems (Cambridge University Press, New York, 2002).

34. P. V. Bulat and K. N. Volkov, One-Dimensional Gas Dynamics Problems and Their Solution Based on High-Resolution Finite Difference Schemes, Nauchno-Tekhn. Vestn. Inform. Tekhnol. Mekhan. Optiki 15 (4), 731–740 (2015).

35. J. D. Regele, J. Rabinovitch, T. Colonius, and G. Blanquart, Numerical Modeling and Analysis of Early Shock Wave Interactions with a Dense Particle Cloud, AIAA Paper (2012).
doi 10.2514/6.2012–3161

Accepted
February 4, 2020